

Imaging real-space flat band localization in kagome magnet FeSn

Authors: Daniel Multer¹, Jia-Xin Yin^{2*}, Md. Shafayat Hossain¹, Xian Yang¹, Brian C Sales³, Hu Miao³, William R Meier⁴, Yu-Xiao Jiang¹, Yaofeng Xie⁵, Pengcheng Dai⁵, Jianpeng Liu⁶, Hanbin Deng², Hechang Lei⁷, Biao Lian^{1*}, M. Zahid Hasan^{1,8,9,10*}

Affiliations:

¹Department of Physics, Princeton University, Princeton, 08544 New Jersey, USA.

²Department of Physics, Southern University of Science and Technology, 518055 Shenzhen, Guangdong, China.

³Materials Science and Technology Division, Oak Ridge National Laboratory, Oak Ridge, 37830 Tennessee, USA.

⁴Materials Science & Engineering Department, University of Tennessee Knoxville, Knoxville, 37921 Tennessee, USA.

⁵Department of Physics and Astronomy, Rice Center for Quantum Materials, Rice University, Houston, 77005 Texas, USA.

⁶School of Physical Science and Technology, ShanghaiTech University, 201210 Shanghai, China.

⁷Department of Physics and Beijing Key Laboratory of Opto-electronic Functional Materials & Micro-nano Devices, Renmin University of China, 100086 Beijing, China.

⁸Lawrence Berkeley National Laboratory, Berkeley, 94720 California, USA.

⁹Princeton Institute for the Science and Technology of Materials, Princeton University, Princeton, 08544 New Jersey, USA

¹⁰Quantum Science Center, Oak Ridge, 37830 Tennessee, USA

†Corresponding authors, E-mail yinjx@sustech.edu.cn; biao@princeton.edu; mzh Hasan@princeton.edu

Kagome lattices host flat bands due to their frustrated lattice geometry, which leads to destructive quantum interference of electron wave functions. Here, we report imaging of the kagome flat band localization in real-space using scanning tunneling microscopy. We identify both the Fe₃Sn kagome lattice layer and the Sn₂ honeycomb layer with atomic resolution in kagome antiferromagnet FeSn. On the Fe₃Sn lattice, at the flat band energy determined by the angle resolved photoemission spectroscopy, tunneling spectroscopy detects an unusual state localized uniquely at the Fe kagome lattice network. We further show that the vectorial in-plane magnetic field manipulates the spatial anisotropy of the localization state within each kagome unit cell. Our results are consistent with the real-space flat band localization in the magnetic kagome lattice. We further discuss the magnetic tuning of flat band localization under the spin-orbit coupled magnetic kagome lattice model.

Introduction

Flat band occurs in quantum systems with localized wave functions, such as the Landau level^{1,2}, heavy fermion compounds³, geometrically frustrated Lieb⁴ and kagome lattices^{5,6} and twisted bilayer graphene^{7,8} *etc.* The research of flat band induced quantum effects can be traced back to the fractional quantum Hall effect^{1,2}. The Landau levels generated by the application of a large magnetic field are perfect electronic flat

bands, and a fractional filling of these flat bands can produce the fractional quantum Hall effect with anyonic excitations. Recently, kagome flat band has been widely discussed in several tantalizing quantum materials⁹⁻¹⁹, exhibiting emergent physics of correlation and topology. However, in these kagome materials, a direct imaging of the flat band localization in real-space as well as its quantum tuning has been lacking.

In this work, we provide a rare example of tunable flat band localization in kagome magnet FeSn. Utilizing high-resolution scanning tunneling microscopy, we observe real-space localization features of the kagome flat band. Through vectorial magnetic field tuning, we further demonstrate the tunability of the flat band localization. Our results advance our microscopic understanding of the flat band localization in a kagome lattice.

Results and discussion

FeSn has a hexagonal structure (space group P6/mmm) with lattice constants^{20,21} $a = 5.3 \text{ \AA}$ and $c = 4.5 \text{ \AA}$. It consists of a Fe₃Sn kagome layer and a Sn₂ honeycomb layer with alternating stacking Fig. 1a. It orders antiferromagnetically below $T_N = 365 \text{ K}$, where the Fe spin moments align ferromagnetically within a single kagome plane but antiferromagnetically from those in the neighboring kagome planes²²⁻²⁶. Kagome flat band (illustrated in Fig. 1b) in FeSn has been evidenced by photoemission data for bulk crystals^{15,27} and planar tunneling data of few-layer thin films²⁸, which is around -0.2eV and arises from the Fe₃Sn layer. Consistent with previous scanning tunneling microscopy study in CoSn family compounds^{14,29-31}, our cryogenic cleaving of FeSn often yields atomic steps with a unit-cell height $\sim 4.5 \text{ \AA}$, either of Fe₃Sn terminations (Fig. 1c for an example) or Sn₂ terminations. Occasionally, we find that Fe₃Sn termination and Sn₂ termination meet at a half-unit cell step edge (Fig. 1d). As the bonding distance in Fe₃Sn layer is much shorter than that of Sn₂, it is more energetically favorable for the Sn₂ layers to be broken during the cleaving process. Based on this fact, there are two features that could help us to identify these two terminations. First, when Sn₂ and Fe₃Sn surface meet at an atomic step edge, the up surface with a step edge should be Sn₂ and the lower integrate surface should be Fe₃Sn. Second, Sn₂ surface should favor (Sn) vacancy impurities while the Fe₃Sn surface should favor (Sn) adatom impurities. These two features collectively help us to identify the two surfaces in Fig. 1d. We further resolve both the Sn₂ and Fe₃Sn lattice layers with atomic resolution as shown in Figs. 1e and f, respectively. The Sn₂ surface clearly exhibit a honeycomb lattice, while we could not resolve further atomic detail of the Fe₃Sn kagome lattice beyond its clear hexagonal lattice symmetry similar to other studies^{9,30}. The atomically identified kagome lattice offers us a unique platform to study the kagome flat band.

Imaging flat band localization

Our angle-resolved photoemission data Fig. 1g as well as its curvature (similar to second derivative method) analysis (Fig. 1h) along a high-symmetry path confirms the existence of flat band near -0.2eV, similar to the existing studies^{15,27,28}. The flatness of the -0.2eV band is reflected in its band width, which is 1 ~ 2 orders of magnitude smaller than other dispersive bands in FeSn. Tunneling spectrum at such high binding energy, however, often combines the local density of states and inelastic tunneling signals, particularly for correlated materials that are rich of bosonic excitations. The tunneling spectrums for Fe₃Sn and Sn₂ lattice layers are displayed in Fig. 1i. The flat band state is expected to be mainly from the kagome lattice layer. This expectation is partially consistent with our observation the there is a broad bump near -0.2eV for the spectrum taken on the Fe₃Sn lattice layer, while no apparent bump is detected near -0.2eV for the Sn₂ honeycomb lattice. We subtract the two spectrums to highlight this difference as in the inset of Fig. 1i. We have been aware that in the planar junction tunneling of few-layer thin films of FeSn (Schottky heterointerface of FeSn and an n-type semiconductor Nb-doped SrTiO₃), a more pronounced flat band peak near -0.2eV is directly detected in the spectrum²⁸. However, we have checked three different crystals with

three different Pt/Ir tips, and our vacuum tunneling on the Fe₃Sn termination does not show a pronounced peak feature near -0.2eV. The reason for this difference remains a mystery for us, which might be related with the surface nature of the flat band (that contributes more to the tunneling spectrum for thin film samples) as well as the different tunneling matrix effects in these two different tunneling experiments.

Focusing on the Fe₃Sn atomic layer, we take spectrums on the Fe atom (that forms kagome lattice) and Sn atom, respectively (Fig. 2a). Their spectral difference also uncovers a pronounced state at -0.2eV (Fig. 2b). For scanning tunneling experiments, as the tip atoms inevitably convolute the local density of states of probing atomic lattices, the detection of such a spectral difference at the flat band energy is remarkable, and hints for spatial localization. dI/dV map at -0.2eV (Fig. 2d) taken on the Fe₃Sn kagome lattice (Fig. 2c) consistently reveal that the corresponding electronic states are localized to the kagome lattice sites. We have checked that with a different tunneling junction set-up as V = -0.1eV and I = 0.1nA, we obtain a similar dI/dV map pattern at V = -0.2eV with states localized to the kagome lattice sites, suggesting that the localization phenomenon does not arise from a junction set-up point effect. dI/dV maps taken at other energies within -0.3eV to +0.3eV (Fig. 2e) do not show such signatures of localized states or show a weaker localization of the kagome lattice (such as the map at energy -0.15V), confirming that the strong electronic localization to kagome lattice is uniquely detected at -0.2eV and agreeing well with our photoemission results. These spectroscopic data taken together support the realization of electron localization of kagome flat band state at -0.2eV. We also note that from data in Figs. 2a and b, the localization phenomenon belongs to a second-order tunneling feature in our data, while the first-order tunneling background can come from the states of other dispersive bands (intrinsic) and the finite spatial resolution of the tip leading to a spatial delocalization in the obtained tunneling data (extrinsic).

Quantum tuning of flat band localization

We further explore the quantum tuning of the flat band localization with a vectorial magnetic field of 1T in Fig. 3(a). It is expected that the magnetic perturbation of the localization will be a third-order tunneling feature in our data, and it should be challenging to detect the corresponding signal. The vector magnetic field has been shown to introduce substantial effects on kagome electrons by scanning tunneling microscopy in several magnetic kagome lattice materials³², which is beyond the capability of the photoemission technique that works under a zero-field condition. Intriguingly, when we apply magnetic field along one of the three *a*-axes for Fe₃Sn, the electronic map at the flat band energy consistently shows a tiny yet detectable intra-unit cell anisotropy (as marked by the colored circles in Fig. 3a), which correlates strongly with the magnetic field direction in all three cases. This observation points to a quantum tuning of the flat band localization, which is likely due to the combination of magnetic field tuned vectorial magnetization (spin reorientation) and strong spin-orbit coupling in the system. The effect is not likely from a simple tip effect, as we find that the anisotropy follows the magnetic field direction that we control rather than a random and fixed anisotropy. Moreover, the magnetic field-controlled spin reorientation is consistent with that reported in kagome magnet Mn₃Sn and Fe₃Sn₂ (Refs. 33-36). The zero field and c-axis field data both show much weaker localization anisotropy in real-space, which is likely due to the canting of spins away from the crystalline a-axis reported earlier^{22,25}. Since the in-plane magnetic field induced anisotropy is most striking, we try to understand its origin based on a spin-orbit coupled magnetic kagome flat band model, which we discuss below.

In a kagome lattice featuring a spin-polarization along the horizontal direction (Fig. 3b), an out-of-plane electric field (from the surface potential) will induce a Rashba spin-orbit coupling, enlarging the hopping of bands not parallel to the horizontal direction. Assume the model without spin-orbit coupling is:

$$H_0 = -t \sum_{\langle i,j \rangle} c_i^\dagger c_j \quad (1)$$

where $\langle i,j \rangle$ stands for the nearest neighbors, c_i^\dagger and c_j are the electron creation and annihilation operators, and $t > 0$ is real. The Rashba spin orbit coupling yields an additional imaginary hopping within each triangular plateau between sublattice sites 1 and 2 (denoted in Fig. 3b), as well as between 1 and 3:

$$H_{SOC} = -i\lambda c_1^\dagger c_2 - i\lambda c_1^\dagger c_3 + h.c. \quad (2)$$

where λ is the spin-orbit coupling strength. After a unitary transformation, rotating all the hopping to real, the total Hamiltonian can be written as:

$$H = -\sum_{\langle i,j \rangle} t_{ij} c_i^\dagger c_j \quad (3)$$

where $t_{ij} = t$ if i and j belong to sublattices 2 and 3, and $t_{ij} = t' = \sqrt{t^2 + \lambda^2}$ if i and j belong to sublattices 1 and 2 or sublattices 1 and 3. In the momentum space, the Hamiltonian is:

$$H(\mathbf{k}) = \begin{bmatrix} 0 & -2t' \cos \mathbf{k} \cdot \mathbf{a}_{12} & -2t' \cos \mathbf{k} \cdot \mathbf{a}_{13} \\ -2t' \cos \mathbf{k} \cdot \mathbf{a}_{12} & 0 & -2t \cos \mathbf{k} \cdot \mathbf{a}_{23} \\ -2t' \cos \mathbf{k} \cdot \mathbf{a}_{13} & -2t \cos \mathbf{k} \cdot \mathbf{a}_{23} & 0 \end{bmatrix} \quad (4)$$

under the momentum basis of the 3 sublattices ($1 >_{\mathbf{k}}$, $2 >_{\mathbf{k}}$, $3 >_{\mathbf{k}}$), where \mathbf{a}_{ij} is the lattice vector from site i to j ($i, j = 1, 2, 3$) in Fig. 3b. The lowest band is the flat band. We further calculate the charge density $\langle n_1 \rangle$, $\langle n_2 \rangle$, and $\langle n_3 \rangle$ on each sublattice site (that are proportional to the local density of states measured in our experiment) as shown in Fig. 3c by setting the system at flat band filling, where $n_i = c_i^\dagger c_i$ is the fermion number operator on site i in Fig. 3b. We find $\langle n_1 \rangle > \langle n_{2,3} \rangle$ when $\lambda \neq 0$, which is consistent with our experimental observations of the geometrical anisotropy of the flat band localization for the kagome lattice layer. Based on this model, we interpret our data as 1) the magnetic field can control the spin direction (magnetization direction) that is consistent with the neutron results^{22,25}; 2) through atomic spin-orbit coupling, the spin orientation affects the charge localization anisotropy.

Conclusion

Physically, the existence of flat band in the maximally symmetric kagome lattice without spin-orbit coupling is indicated by the presence of localized eigenstates on a hexagon as illustrated in Fig. 3d, which has amplitudes with alternating sign, such that any amplitudes outside the hexagon induced by the hopping cancel perfectly. For the Rashba spin-orbit coupled magnetic kagome lattice with horizontal spin-polarization considered here, strictly localized eigenstates no longer exist, since the hoppings along the three directions are no longer equal. However, there still exists one-dimensional eigenstates localized on each horizontal line of bonds parallel to the spin-polarization, with alternating sign of amplitudes as illustrated in Fig. 3e. This is because the electron hoppings not parallel to the spin direction are still equal in magnitude and thus cancel with each other. These eigenstates are thus extended (localized) in the parallel (perpendicular) direction to the spin polarization. We expect this magnetization-controlled localization anisotropy physics can be further explored by future transport, spectroscopy and scattering experiments for kagome magnets made into thin films.

References:

[1] D. C. Tsui, H. L. Stormer & A. C. Gossard. Two-dimensional magnetotransport in the extreme quantum limit. *Phys. Rev. Lett.* **48**, 1559–1562 (1982).

[2] R. B. Laughlin. Anomalous quantum Hall effect: an incompressible quantum fluid with fractionally charged excitations. *Phys. Rev. Lett.* **50**, 1395–1398 (1983).

- [3] Q. Si & F. Steglich. Heavy fermions and quantum phase transitions. *Science* **329**, 1161–1166 (2010).
- [4] E. H. Lieb. Two theorems on the Hubbard model. *Phys. Rev. Lett.* **62**, 1201 (1989).
- [5] R. L. Johnston & R. Hoffmann. The kagomé net: Band theoretical and topological aspects. *Polyhedron* **9**, 1901-1911 (1990).
- [6] Mielke, A. Ferromagnetic ground states for the Hubbard model on line graphs. *J. Phys. A* **24**, L73 (1991).
- [7] R. Bistritzer & A. H. MacDonald. Moiré bands in twisted double-layer graphene. *Proc. Natl Acad. Sci. USA* **108**, 12233–12237 (2011).
- [8] Cao, Y. et al. Unconventional superconductivity in magic-angle graphene superlattices. *Nature* **556**, 43–50 (2018).
- [9] Z. Lin et al. Flatbands and emergent ferromagnetic ordering in Fe₃Sn₂ kagome lattices. *Phys. Rev. Lett.* **121**, 096401 (2018).
- [10] J. -X. Yin et al. Negative flat band magnetism in a spin–orbit-coupled correlated kagome magnet. *Nat. Phys.* **15**, 443–448 (2019).
- [11] M. Kang et al. Dirac fermions and flat bands in the ideal kagome metal FeSn. *Nat. Mater.* **19**, 163–169 (2020).
- [12] S. S. Zhang et al. Many-body resonance in a correlated topological kagome antiferromagnet. *Phys. Rev. Lett.* **125**, 046401 (2020).
- [13] Z. H. Liu et al. Orbital-selective Dirac fermions and extremely flat bands in frustrated kagome-lattice metal CoSn. *Nature Communications* **11**, 4002 (2020).
- [14] J. X. Yin et al. Fermion–boson many-body interplay in a frustrated kagome paramagnet *Nature Communications* **11**, 4003 (2020).
- [15] M. Kang et al. Topological flat bands in frustrated kagome lattice CoSn. *Nature Communications* **11**, 4004 (2020).
- [16] W. R. Meier et al. Flat bands in the CoSn-type compounds. *Phys. Rev. B* **102**, 075148 (2020).
- [17] M. Li et al. Dirac cone, flat band and saddle point in kagome magnet YMn₆Sn₆. *Nat. Commun.* **12**, 3129 (2021).
- [18] H. Huang et al. Flat-band-induced anomalous anisotropic charge transport and orbital magnetism in kagome metal CoSn. *Phys. Rev. Lett.* **128**, 096601 (2022).
- [19] Y. Yu et al. Topological surface states and flat bands in the kagome superconductor CsV₃Sb₅. *Science Bulletin.* **67**, 495-500 (2022).
- [20] W. F. Ehret & A. F. Westgren. x-Ray Analysis of Iron-Tin Alloys. *J. Am. Chem. Soc.* **55**, 1339 (1933).
- [21] H. Giefers and M. Nicol. High pressure X-ray diffraction study of all Fe-Sn intermetallic compounds and one Fe-Sn solid solution. *J. Alloys and Compds.* **422**, 132 (2006).
- [22] K. Yamaguchi & H. Watanabe. Neutron diffraction study of FeSn. *J. Phys. Soc. Jpn.* **22**, 1210–1213 (1967).

- [23] S. K. Kulshreshtha & P. Raj. Anisotropic hyperfine fields in FeSn by Mossbauer spectroscopy. *J. Phys. F: Met. Phys.* **11**, 281–291 (1981).
- [24] B. C. Sales et al. Electronic, magnetic, and thermodynamic properties of the kagome layer compound FeSn. *Phys. Rev. Mater.* **3**, 114203 (2019).
- [25] Y. Xie et al. Spin excitations in metallic kagome lattice FeSn and CoSn. *Commun Phys* **4**, 240 (2021).
- [26] S-H. Do et al. Damped Dirac magnon in the metallic kagome antiferromagnet FeSn. *Phys. Rev. B* **105**, L180403 (2022).
- [27] Z. Lin et al. Dirac fermions in antiferromagnetic FeSn kagome lattices with combined space inversion and time-reversal symmetry. *Phys. Rev. B* **102**, 155103 (2020).
- [28] M. Han et al. Evidence of two-dimensional flat band at the surface of antiferromagnetic kagome metal FeSn. *Nat Commun* **12**, 5345 (2021).
- [29] J-X. Yin et al. Discovery of charge order and corresponding edge state in kagome magnet FeGe. *Phys. Rev. Lett.* **129**, 166401 (2022).
- [30] H. Li et al. Spin-polarized imaging of the antiferromagnetic structure and field-tunable bound states in kagome magnet FeSn. *Sci Rep* **12**, 14525 (2022).
- [21] Lee, S-H. et al. Spin-polarized and possible pseudospin-polarized scanning tunneling microscopy in kagome metal FeSn. *Commun Phys* **5**, 235 (2022).
- [32] J-X. Yin, S-H. Pan & M. Z. Hasan, M. Probing topological quantum matter with scanning tunnelling microscopy. *Nat Rev Phys* **3**, 249–263 (2021).
- [33] S. Tomiyoshi & Y. Yamaguchi. Magnetic structure and weak ferromagnetism of Mn₃Sn studied by polarized neutron diffraction. *J. Phys. Soc. Jpn* **51**, 2478–2486 (1982)
- [34] S. Nakatsuji, N. Kiyohara & T. Higo. Large anomalous Hall effect in a non-collinear antiferromagnet at room temperature. *Nature* **527**, 212–215 (2015).
- [35] J. X. Yin et al. Giant and anisotropic many-body spin–orbit tunability in a strongly correlated kagome magnet. *Nature* **562**, 91–95 (2018).
- [36] Y. Li et al. Magnetic-field control of topological electronic response near room temperature in correlated kagome magnets. *Phys. Rev. Lett.* **123**, 196604 (2019).

Methods

Single crystals of FeSn are grown out of a Sn flux. 34 g of Sn and 0.33 g of Fe are loaded into a 10-cc alumina crucible and sealed in a silica ampoule under vacuum. The ampoule is heated to 1100 °C, soaked for 12 h, cooled to 1000 °C and soaked for 48 h with occasional shaking of the ampoule, cooled to 800 °C at 6 °C/h, and then cooled to 600 °C at 1 °C/h. Near 600 °C the excess Sn flux is centrifuged into another 10-cc crucible filled with quartz wool.

Single crystals with a size up to 2mm × 2mm are cleaved in situ at 77K in ultra-high vacuum conditions and then inserted into the microscope head, already at ⁴He base temperature (4.2K). Topographic images in this work are taken with the tunneling junction set-up $V = -100\text{mV}$ and $I = 0.05\text{nA}$. Tunneling

conductance spectra are obtained with an Ir/Pt tip using standard lock-in amplifier techniques with a lock-in frequency of 1003.3Hz and a junction set-up of $V = -300\text{mV}$, $I = 1\text{nA}$, and a root mean square oscillation voltage of $V_m = 1\text{mV}$. Tunneling conductance maps are obtained by taking dI/dV spectrums at each pixel position with a junction set-up of $V = -300\text{mV}$, $I = 0.4\text{nA}$, and a root mean square oscillation voltage of 10mV .

We estimate the possible renormalization factor for dI/dV spectra taken at different spatial positions. The measured step height of the Sn_2 layer is 1.8\AA , which is smaller than that in the bulk crystal structure $\sim 2.2\text{\AA}$. One possible reason is that there are variations of the bond distances at the surface, as an extrinsic surface effect. Another possible reason for this difference $L = -0.4\text{\AA}$ is that the Fe_3Sn layer has much larger local density of states that make the sample-tip height higher even under the same tunneling current and voltage as that in the Sn_2 layer, which is noted as an intrinsic effect related to the quantum tunneling principle. The tunneling current is $I \sim \exp(-2\kappa L)$, where κ is a work function related coefficient with a typical value of 1\AA^{-1} and L is the sample tip distance. Under the assumption that the step height difference is purely caused by the density states difference, then the renormalization factor for the dI/dV spectrum on the Fe_3Sn surface relative to that on the Sn_2 surface can be estimated as $\exp(-2\kappa L) \sim \exp(0.8) = 2.2$. In a similar spirit, on the Fe_3Sn surface, the measured height between Fe site and Sn site is 0.08\AA , while their atomic radius difference is estimated as -0.07\AA . Accordingly to this height difference $= -0.15\text{\AA}$ and under the assumption that there is no surface structure reconstruction, the renormalization factor for the dI/dV spectrum at the Fe site relative to that on the Sn site on the same Fe_3Sn surface can be estimated as $\exp(-2\kappa L) \sim \exp(0.3) = 1.3$. We note that while our estimation provides a clue on how Fe atom can feature more density of states near the Fermi level than that on the Sn atom, we have made strong assumptions on the surface structure condition, work function, and atomic radius that would need further experimental confirmation in future.

Acknowledgement

M.Z.H. acknowledges support from the US Department of Energy, Office of Science, National Quantum Information Science Research Centers, Quantum Science Center and Princeton University; visiting scientist support at Berkeley Lab (Lawrence Berkeley National Laboratory) during the early phases of this work; support from the Gordon and Betty Moore Foundation (GBMF9461); and support from the US DOE under the Basic Energy Sciences programme (grant number DOE/BES DE-FG-02-05ER46200) for the theory and angle-resolved photoemission spectroscopy work. B.L. is supported by the Alfred P. Sloan Foundation, the National Science Foundation through Princeton University's Materials Research Science and Engineering Center DMR-2011750; and the National Science Foundation under award DMR-2141966. J.-X.Y. acknowledges support from South University of Science and Technology of China principal research grant (number Y01202500). H.L. was supported by National Key R&D Program of China (Grants Nos. 2018YFE0202600 and 2022YFA1403800), Beijing Natural Science Foundation (Grant No. Z200005), National Natural Science Foundation of China (Grants Nos. 12274459). Work at Oak Ridge National Laboratory was sponsored by the U.S. Department of Energy, Office of Science, Basic Energy Sciences, Materials Sciences and Engineering Division. Work at Rice University was supported by US NSF-DMR-2100741 and by the Robert A. Welch Foundation under grant no. C-1839.

Author contributions

D.M., J.-X.Y., M.S.H. and X.Y. performed the spectroscopic experiment with contributions from H.M., Y.-X.J., Y.X., P.D., J.L. and H.D. in consultation with M.Z.H. B.C.S., W.R.M. and H.L. provided the samples. B.L. provided the theoretical analysis in consultation with J.-X.Y. and M.Z.H. J.X.Y., B.L. and M.Z.H. wrote the paper and discussed the paper with all authors.

Competing interests

The authors declare no competing interests.

Figures

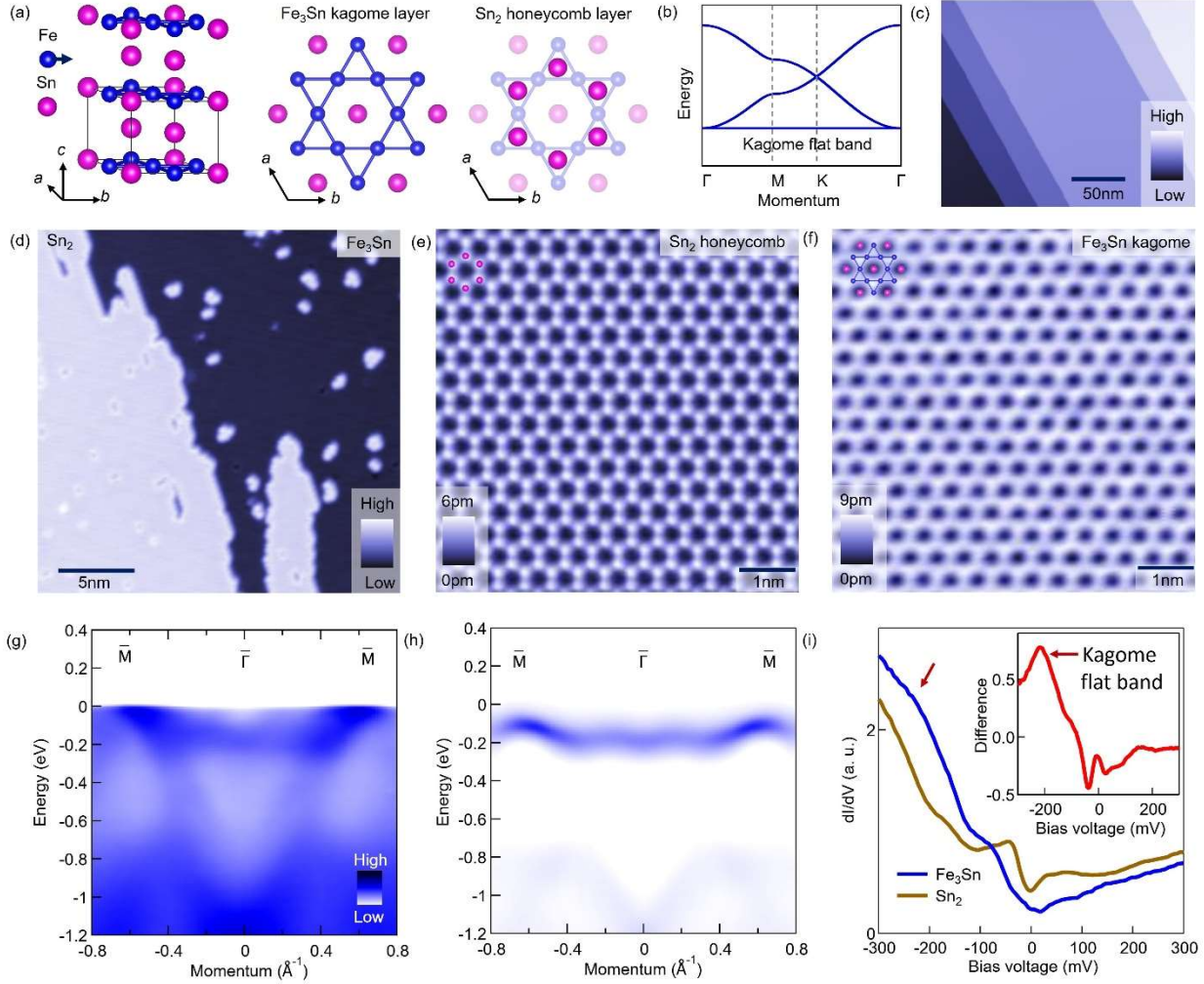


Fig. 1 Flat band in kagome magnet FeSn. (a) Crystal structure of FeSn, which is composed of a Fe_3Sn lattice layer and a Sn_2 lattice layer. (b) Fundamental band structure based on a tight-bind model in a kagome lattice considering nearest neighboring electron hopping. (c) A topographic image consists of unit-cell steps (Fe_3Sn lattice layers). Data taken with $V = -100\text{mV}$ and $I = 0.05\text{nA}$. (d) A topographic image consists of Fe_3Sn and Sn_2 lattice layers ($V = -100\text{mV}$, $I = 0.05\text{nA}$). (e) Atomically resolved topographic image of Sn_2 honeycomb lattice ($V = -100\text{mV}$, $I = 0.1\text{nA}$). The inset marks the Sn atoms. (f) Atomically resolved topographic image of Fe_3Sn kagome lattice ($V = -100\text{mV}$, $I = 0.1\text{nA}$). The inset marks the Fe and Sn atoms. (g) Angle-resolved photoemission intensity plot for the electron band. Data taken with photon energy of 90eV and temperature of 10K . (h) Symmetrization (along momentum direction) and curvature analysis (along energy direction) of the photoemission data, highlighting the flat band around -0.2eV . (i) Tunneling spectrums taken on Fe_3Sn and Sn_2 lattice layers, respectively ($V = -300\text{mV}$, $I = 1\text{nA}$, $V_m = 1\text{mV}$). Each spectrum is obtained through averaging spectrums taken over an area of $2\text{nm} \times 2\text{nm}$. The inset shows the subtraction of Fe_3Sn spectrum by the Sn_2 spectrum, highlighting a peak around -0.2eV as a candidate signature of kagome flat band state.

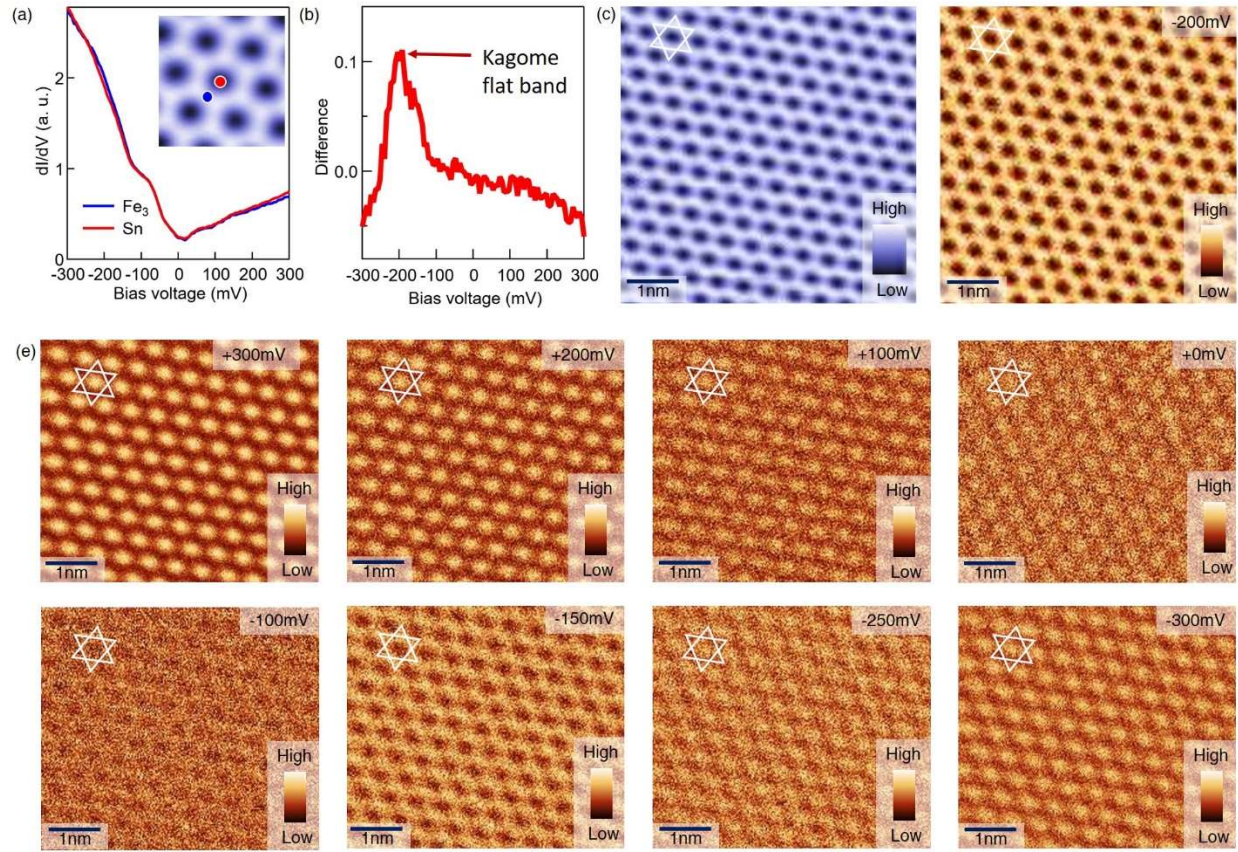


Fig. 2 **Imaging flat band localization.** (a) Tunneling spectrum taken on the Fe and Sn atom sites of the Fe_3Sn kagome layer (as illustrated in the inset), respectively ($V = -300$ mV, $I = 1$ nA, $V_m = 1$ mV). (b) The subtraction of the above two spectrums, highlighting a peak around -0.2 eV as a candidate signature of kagome flat band state. (c) Topographic image of a Fe_3Sn kagome lattice ($V = -300$ mV, $I = 0.4$ nA). The white lines denote the kagome lattice. (d) Corresponding dI/dV map taken at -0.2 eV, showing electronic states localized to the kagome lattice ($V = -300$ mV, $I = 0.4$ nA, $V_m = 10$ mV). The white lines denote the kagome lattice. (e) A series of dI/dV maps taken from $+0.3$ eV to -0.3 eV, respectively, showing a striking contrast with the -0.2 eV map ($V = -300$ mV, $I = 0.4$ nA, $V_m = 10$ mV). The white lines denote the kagome lattice for each map.

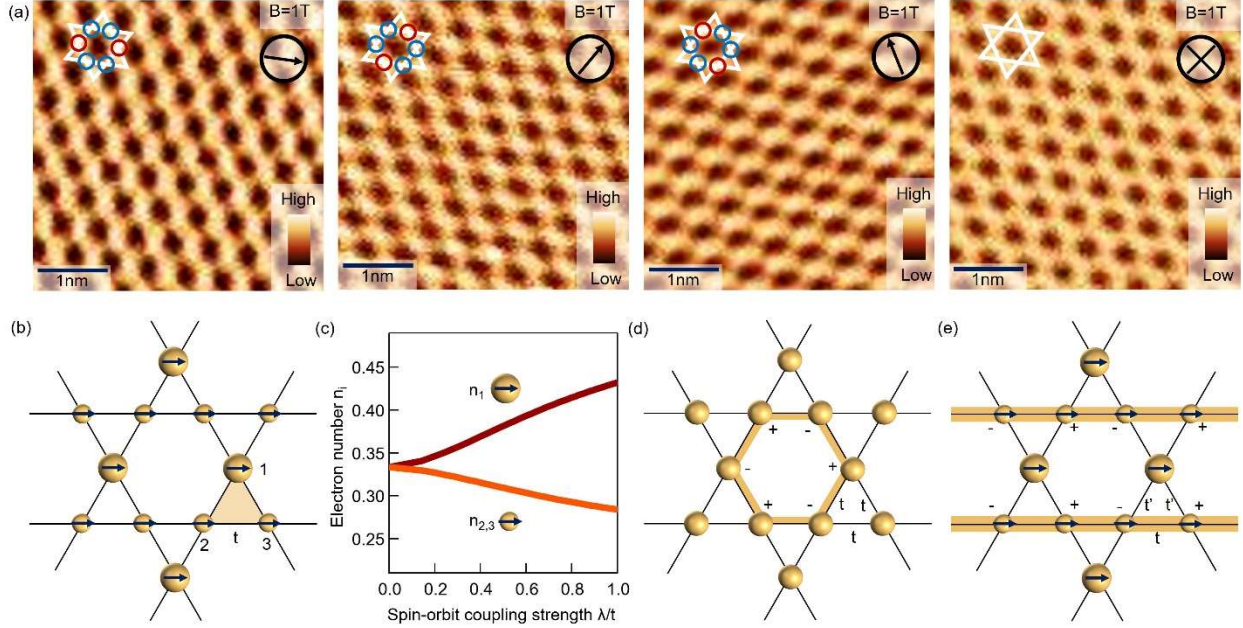


Fig. 3 Quantum tuning of flat band localization. (a) dI/dV maps taken at -0.2eV on the Fe_3Sn kagome lattice with in-plane and out-of-plane magnetic fields of 1T ($V = -300\text{mV}$, $I = 0.4\text{nA}$, $V_m = 10\text{mV}$). The in-plane magnetic field cause spatial anisotropy of the electronic state within each kagome unit cell (marked by the circles with different colors within each kagome pattern draw by white lines), which correlates strongly with the magnetic field direction. The red circles mark the local intensity related with $\langle n_1 \rangle$, and the blue circles mark the local intensity related with $\langle n_2 \rangle$ or $\langle n_3 \rangle$. (b) Electron number distribution based on a kagome lattice model, which provides an explanation of our experiments. This model considers atomic spin-orbit coupling, ferromagnetic order with spins along the horizontal direction, and flat band electron filling. (c) The charge density anisotropy as a function of spin-orbit coupling strength under the kagome flat band model. (d) The plus and minus signs denote the amplitude of a localized kagome flat band eigenstate. Electron hopping amplitudes outside the golden hexagon are canceled by the destructive quantum interference, leading to the two-dimensional electron localization. (e) In the Rashba spin-orbit coupled magnetic kagome lattice with horizontal spin-polarization, there exist one-dimensional eigenstates localized on each horizontal golden line of bonds, which have alternating signs of amplitude, such that the electron hopping amplitudes perpendicular to the spin direction still cancel with each other.